Thermal analysis of a lithium-ion pouch cell under aggressive automotive duty cycles with minimal cooling

D. Worwood*, E. Hosseinzadeh*, Q. Kellner*, J. Marco**, D. Greenwood*, R. McGlen†, W. D. Widanage*, A. Barai*, P. Jennings*

*Warwick Manufacturing Group, University of Warwick, Coventry, UK,***e-mail: james.marco@warwick.ac.uk,* †Thermacore Europe, Ashington, UK

Keywords: Automotive battery, thermal management, thermal modelling, minimal cooling, performance EV

Abstract

The performance and ageing of lithium-ion cells are particularly sensitive to the battery operating temperature and in-cell temperature gradient. To mitigate adverse ageing whilst maximising performance, thermal management systems are required to maintain the cell operating temperature within its optimum range. In this paper, an aggressive duty cycle representative of track racing conditions for a performance electric vehicle (EV) is used as an input into a 1-D electrochemical-3-D thermal model which is validated against experimental data with a peak error of 10.6%. The simulated temperature response of the cell during the duty cycle is analysed under 4 minimal cooling conditions. The results indicate that natural convection with air is ineffective in limiting the peak cell temperature rise during the cycle to 20 ℃ and a more involved cooling method is necessary.

1 Introduction

Lithium-ion pouch type batteries as an energy storage solution for electric vehicles (EVs), plug-in hybrid electric vehicles (PHEVs) and hybrid electric vehicles (HEVs) are being increasingly employed by a number of Original Equipment Manufacturers (OEMs) [1], partially owing to their superior packing density and lightweight design [2]. Further benefits of large format pouch designs include the potential for greater cost reduction as economies of scale are reached when compared to that attainable with the current more mature 18650 cylindrical cell format [3].

As with other lithium-ion battery formats, the performance and ageing rates of pouch type lithium-ion batteries are sensitive to both the battery operating temperature [4] and in cell-temperature gradient [5]. Past research has shown that the cell ageing rate follows an Arrhenius type rate law [6] with higher temperatures accelerating the rate of the parasitic reaction between the electrolyte and anode particles, leading to growth of the solid-electrolyte interface (SEI) layer and a subsequent irreversible loss in cell capacity [7]. Low temperatures, however, impede the rate of electrochemical reactions within the cell thus affecting performance. Whilst chemistry dependant, temperatures below circa 20 ℃ have been reported [4], [8] to reduce the usable cell capacity. As such, given the balance between performance and reduced ageing, an optimum operating temperature exists for lithium-ion cells between circa 20 ± 5 ℃.

Temperature gradients existing within the cell govern the value for the localised cell internal resistance, with higher temperatures decreasing the resistance value from improved mass transport [9]. Hotter areas of the cell therefore exhibit an increase in localised current density relative to colder areas where the mass transport rate is lowered. Such inhomogeneities in current density have be shown through simulation by Fleckenstein et al. [10] to cause an imbalance of 8% in the cell state of charge (SOC) throughout the cell material when a 20 ℃ in-cell temperature gradient exists. Yang et al. [11] further highlighted that inhomogeneities in SOC between cells within a parallel string induce unbalanced ageing effects across the string. Specifically, the capacity loss was observed to increase in an approximate linear fashion as the maximum temperature gradient between the cells increased, with the effect intensifying at higher battery operating temperatures. On the cell-level, Troxler et al. [5] theorised that layers within the cell can be considered as connected in parallel with one another, with temperature gradients leading to localised ageing and exasperating the overall ageing rate of the cell. They observed experimentally that the behaviour of the cell under an imposed temperature gradient was representative of a characteristic temperature higher than the volume average temperature of the cell, with larger gradients increasing the departure towards a higher characteristic operating temperature than that of the volume averaged temperature. Owing to this, temperature gradients throughout the cells and between cells within the pack should aim to be kept to below circa 5 ℃ [11], [12].

Given the importance of temperature control, thermal modelling approaches [13]–[15] are commonly employed to estimate the temperature performance of lithium-ion cells under a given electrical loading condition alongside experimental measurements as part of the design strategy for the thermal management system [16]. Common approaches to define the performance of the baseline thermal management strategy - i.e. cell without active cooling/ minimal thermal management consideration – analyse the cell temperature response when subject to a constant charge/discharge as in [17]–[21]. A lesser amount of available literature appears to

exist for the cell temperature response with minimal cooling when subject to an aggressive duty cycle scenario, an example of which is in [12]. Other studies have been undertaken for the cell temperature response under aggressive duty cycles such as the US06 cycle, however, these are under active cooling conditions [22]. There therefore exist a lack of literature on the temperature response of a pouch cell subject to a highly aggressive duty cycle under minimal cooling conditions.

In this paper, the temperature response of a lithium-ion pouch cell subject to an extreme duty cycle characteristic of a performance EV is analysed through use of a coupled electrochemical-thermal model to determine a potential realistic worst case thermal condition for the cell under minimal thermal management considerations for this application. Section 2 outlines the model development of the electrochemical and thermal models together with a brief discussion on the development of the aggressive duty cycle. Validation of the coupled electrochemical-thermal model against experimental temperature measurements from the test high power pouch cell is discussed in Section 3. In Section 4, the thermal response of the cell under the duty cycle is compared to that under constant discharge conditions at high C-rates to asses which electrical loading condition incurs the largest in cell temperature gradient and maximum cell temperature rise under 4 minimal cooling conditions that may exist within a battery pack with little to no thermal management consideration.

2 Model development

2.1 1-D electrochemical battery model

The 1-D electrochemical model considers a single cell sandwich structure comprised of the negative current collector (copper), negative electrode (graphite), separator layer (polypropylene), positive electrode ($LiFePO_4$) and positive current collector layer (aluminium). The electrode layers are assumed to comprise spherical solid particles mixed with liquid electrolyte forming a porous material. A list of the governing 1-D electrochemical equations can be found in [23], which to summarise, includes the electrochemical reaction kinetics, ion transport and charge conservation in the electrolyte and solid particle phases and the material balance for lithium-ions in the electrolyte and solid phases.

The heat generation within the battery is derived from the general battery energy balance as presented by Bernardi et al. [24] which is expressed as:

$$Q = I(U_{ocv} - V) - IT\frac{dU_{ocv}}{dT} \quad (1)$$

Where Q is the total battery heat generation rate [W], I the battery cell current [A], U_{ocv} the battery open circuit voltage [V], V the battery cell potential [V] and T the battery temperature [K]. The battery temperature is calculated from the simplified battery energy balance as a function of time by:

$$MC_p^m\frac{dT}{dt} = Q - hA(T - T_\infty) \quad (2)$$

Where M is the mass of the battery [kg], h the convective heat transfer coefficient [$W.m^{-2}.K^{-1}$], A the surface area for heat transfer [m^2], C_p^m the mean heat capacity of the battery and T_∞ the temperature of the bulk heat transfer medium [K]. The electrochemical equations, Eq.(1) and (2) are used to solve for the battery heat generation in the battery under the assumption of homogenous battery temperature and hence uniform battery heat generation. COMSOL Multiphysics is used as the solution package.

2.2 3-D bulk thermal model

The heat generation output from the coupling of the electrochemical model with the simplified battery energy balance is used as an input into the 3-D thermal model which considers the cell material as one homogenous layer displaying anisotropic thermal conductivity. The full 3-D energy balance for the cell bulk material is given by:

$$\rho C_p^m\frac{\partial T}{\partial t} = q''' + \frac{\partial}{\partial y}\left(k_y\frac{\partial T}{\partial y}\right) + \frac{\partial}{\partial z}\left(k_z\frac{\partial T}{\partial z}\right) + \frac{\partial}{\partial x}\left(k_x\frac{\partial T}{\partial x}\right) \quad (3)$$

Where ρ is the effective battery density [$kg.m^{-3}$], q''' the volumetric battery heat generation rate [$W.m^{-3}$] and k_y, k_x, k_z the effective battery thermal conductivity in the y, x and z directions respectively [$W.m^{-1}.K^{-1}$]. Newton's law of cooling is applied as the boundary condition for each surface. The battery tabs are modelled using the approach by Wu et al. [25] which considers the protruding current collector layers from the top of the cell to fold into an extruded triangle as the base of the tab. The model representation of the cell used for the thermal modelling is viewable in Figure 1. The joule heating within the cell tabs is also described using the approach in [25].

Table 1: Thermal and physical properties of battery cell

C_p^m [$J.kg^{-1}.K^{-1}$]	ρ [$kg.m^{-3}$]	$k_y = k_z$ [$W.m^{-1}.K^{-1}$]	k_x [$W.m^{-1}.K^{-1}$]
1114	1884	30	0.284

Thermal and physical properties for the battery cell used in the model are shown in Table 1. Values for k_x and C_p^m are taken from experimental measurements conducted by Vertiz et al. [15] on a pouch type $LiFeP0_4$ battery cell. Values for k_y and k_z are taken from [26]. The effective cell density was calculated form the volume of the battery and its weighed mass.

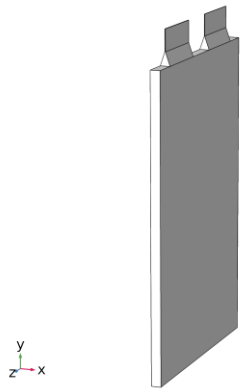

Figure 1: 3-D battery cell COMSOL model

2.3 Aggressive duty cycle

Twelve popular racing tracks varying in length, location and racing class, an electric sports car powered by two electric machines and an aggressive driver were modelled and parameterized in the IPG CarMaker software suite. The race tracks were modelled based on satellite images, and the data for the motor model was provided by an industrial partner. Regenerative braking was set up to be used in sequential order meaning mechanical brakes would only be applied when peak charging power is achieved. Traction battery input and output power was limited to 270 kW. A track driving simulation was run for each track and the duty cycles at the battery pack terminals were recorded [27]. Subsequently, the data was normalised and a mean lap for each circuit was determined. The mean lap for each track was analysed in terms of their amplitude spectra and histograms. Visual inspection revealed similarities for the majority of the tracks. An average power spectrum and histogram in the form of an inverse cumulative distribution function was determined and the generic duty cycle was developed using an algorithm described in [28].

3 Thermal model validation

The thermal model is compared against temperature measurements taken from a test $LiFePO_4$ pouch cell subject to 1C, 3C and 5C continuous discharge conditions. The test cell has been placed in a climate chamber that circulates air at 20 ℃, whereby the cell is suspended such that each surface is exposed to free movement of air. A value of 10 $W.m^{-2}.K^{-1}$ is chosen for each cell surface and tabs to represent natural convection conditions within the climate chamber. Seven thermocouples were distributed across the surface of the test cell giving large coverage to capture the surface temperature evolution during discharge. Figure 2 compares the evolution of the maximum cell surface temperature outputted from the 3-D thermal model against the highest experimental temperature reading from the test cell for each discharge condition. The peak error between the model and test cell is calculated as 10.6%, 10.2% and 10.4% for the 1C, 3C and 5C discharge condition respectively. The assumption of a static h value may contribute to the error in the model, together with the assumed values for the electrochemical and thermal parameters.

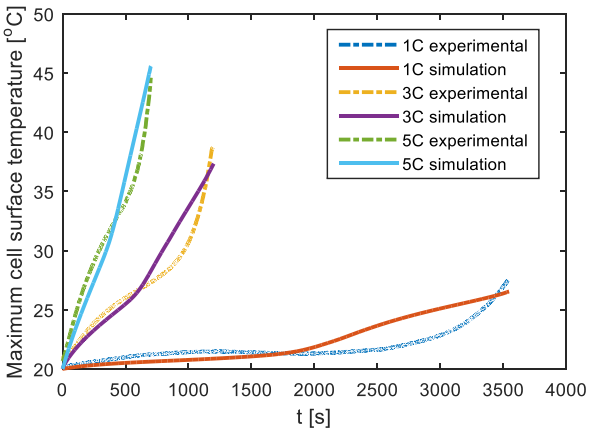

Figure 2: Comparison between 3-D thermal model and measured experimental cell maximum surface temperature

4 Analysis

The results for the aggressive duty cycle are shown in Figure 3 with a time step resolution of 1s, which was chosen to enable the 3-D thermal model to run within the limit of 64 GB computational RAM. Here the normalised outputs from the model are multiplied by the maximum allowable C-rate of the battery during both instances of charge (positive) and discharge (negative), which for the modelled cell used in this analysis is 8C for discharge and 3C for charge.

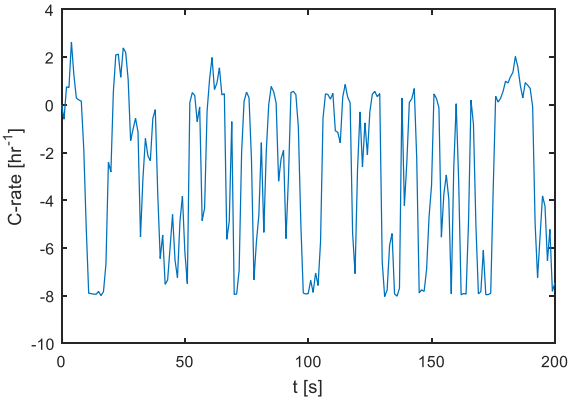

Figure 3: Aggressive duty cycle for a performance EV

The temperature response of the cell subject to the duty cycle is assessed as a function of 4 minimal cooling conditions. The first considers zero heat transfer, whereby each battery surface and tabs has a h value of 0. On the pack level, this may represent a fully insulated battery pack with no cooling or circulation of air from natural convection. The second considers moderate natural convection with a h value of 10 $W.m^{-2}.K^{-2}$ [29] at only the top surface of the cell and at the tabs, reflecting exposure to the free movement of air with ventilation. The sides, bottom, front and back faces of the cell are insulated which would represent a battery pack with side insulation and no spacing between cells blocking air passage. The third conditions considers a lower value for h under natural convection of 5 $W.m^{-2}.K^{-2}$ (similar to that used in [13]) at all the cell surfaces and tabs bar the base of the cell which is insulated. This may represent a poorly ventilated pack which

has a degree of spacing between cells and the module housing to allow for air passage between and around the sides of the cell. The fourth condition is similar to the third albeit that the natural convection h value is higher at 10 $W.m^{-2}.K^{-2}$ which may be representative of a pack with improved ventilation. The minimal cooling cases considered for the cell thermal analysis are summarised in Table 2.

Table 2: Minimal thermal management cases

Case no.	h value at cell sides, back and front [$W.m^{-2}.K^{-1}$]	h value at cell top and tabs [$W.m^{-2}.K^{-1}$]	Potential pack level minimal thermal management strategy
1	0	0	Fully insulated pack with no ventilation
2	0	10	Ventilated cell top and tabs
3	5	5	Spacing around cells with poor air ventilation
4	10	10	Spacing around cells with improved air ventilation

An example of the heat generation profile output from the electrochemical model and coupled simplified battery energy balance is shown in Figure 4 for Case 4. Here the duty cycle is looped back-to-back 4 times. The time averaged value across the 4 cycle loops is 1.03×10^5 $W.m^{-3}$, which given the volume of the battery (excluding tabs) is 27.1W.

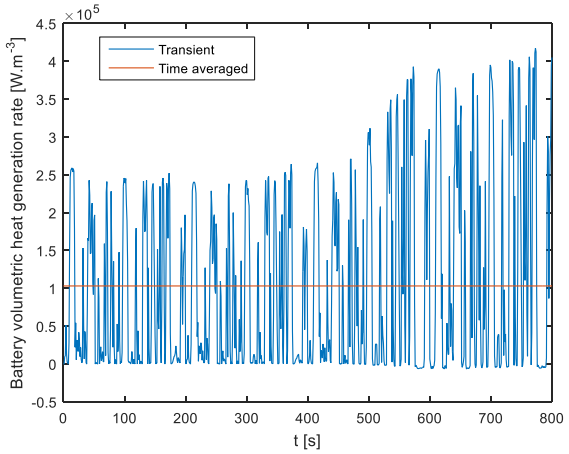

Figure 4: Battery volumetric heat generation profile during 4 loops of the aggressive duty cycle for Case 4

The variation in heat generation rate across each loop of the duty cycle is due to the varying SOC within the battery, which affects the value of the heat generation rate as calculated from the coupled electrochemical-simplified battery energy balance model.

4.1 Battery cell temperature response

Results from the 3-D thermal model as a function of electrical loading condition and cooling case are shown in Figure 5. In each subplot, the transient evolution of the maximum (T_{max}), minimum (T_{min}) and volume averaged (T_{avg}) temperature of the cell material (excluding tabs) is plotted for the duty cycle and constant 8C and 3C discharge cases. The constant discharges are performed from 100-0% SOC, where the duty cycle initial SOC is set at 90%. The temperature of the bulk air heat transfer medium and initial cell temperature profile is set at 20 ℃.

During Case 1, the maximum temperature of the battery cell reaches 70.15 ℃, 54.92 ℃ and 48.23 ℃ at the end of the 8C, duty cycle and 3C discharge condition respectively. The sawtooth type evolution of T_{max} for the duty cycle is due to the transient tab heat generation arising from the transient current profile, which enables the hot spot temperature near the base of the positive tab to cool slightly via heat conduction into cooler regions of the cell below the tab during instances where the tab current throughout decreases. As the degree of cooling on the cell increases for each cooling case, the temperature rise of the cell decreases. For Case 2 with uneven tab cooling, T_{max} for the duty cycle reduces to 52.34 ℃. Case 3 and 4 which allow for cooling on the larger surface area faces of the cell (front and back) enable T_{max} to decrease more significantly. For the duty cycle, T_{max} at the end is reduced to 48.13 ℃ and 43.31 ℃ for Case 3 and 4 respectively. The greater reduction in T_{max} from enabling air passage on the large faces of the cell than compared to uneven tab cooling highlights the importance of accommodating spacing between cells within the pack as a thermal management provision for reducing the cell T_{max}. However, all of these minimal cooling approaches are inadequate in maintaining the cell temperature to below 40 ℃ at the end of the 4 duty cycle loops, raising issues over enhanced cell ageing [9].

The maximum cell temperature gradient (ΔT_{max}) at the end of each electrical loading condition (t_{final}) is summarised in Table 3.

Table 3: Maximum cell temperature gradient values at t_{final}

Case	$\Delta T_{max} = T_{max} - T_{min}$ [℃]		
	3C	8C	Duty cycle
1	0.784	4.41	2.87
2	3.23	4.35	2.59
3	1.68	4.19	2.49
4	2.35	4.67	2.60

For the 8C discharge and duty cycle, the maximum temperature gradient remains relatively unaffected between cooling cases. Introducing uneven cell cooling at the tabs in Case 2 results in a slight decrease in ΔT_{max} for 8C and the duty cycle, however, for 3C the uneven tab cooling increases ΔT_{max} by 312%. This difference is attributed to the higher level of tab heat generation and hence greater heat rejection rate into the cell present during the 8C discharge and duty cycle owing to the higher tab current throughputs than compared to 3C where the current is lower.

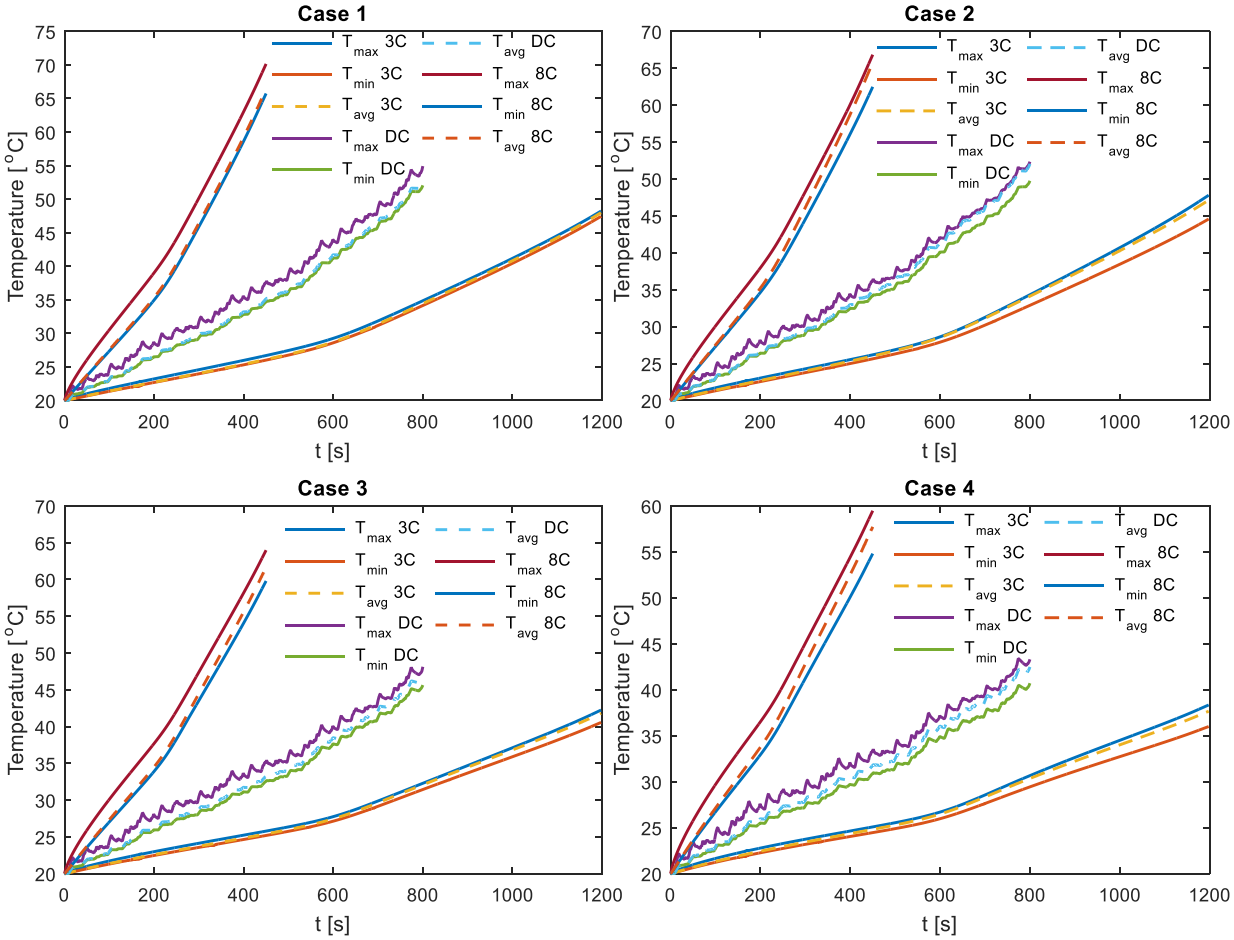

Figure 5: Simulated thermal response of the cell as a function of the electrical loading condition and degree of cooling

Specifically, the tab heat generation rate for the negative and positive tabs is 0.594 W and 1.80 W respectively for 8C, but only 0.0835 W and 0.252 W respectively for 3C. The higher tab heat generation therefore governs the cell ΔT_{max} under Case 2 for the duty cycle and 8C electrical loading conditions, where for 3C discharge, the uneven tab cooling at the top of the cell governs the cell ΔT_{max}. Similar results have been reported by Bazinski and Wang [30] who report a benefit for tab cooling at high C-rates (8C) but can exasperate cell temperature gradients when applied at lower C-rates (3C). Figure 6 displays the temperature profile across the cell from the front and side view for 8C at t_{final} during cooling Case 4, highlighting the effect of the tab heat generation on the cell ΔT_{max}.

For cooling Case 3, introducing even cooling around the cell reduces ΔT_{max} by 47.7% for 3C relative to Case 2. However, increasing the intensity of the even cooling in Case 4, increases ΔT_{max} by 39.9% relative to Case 3 for the 3C discharge. A similar trend is observed for 8C and the duty cycle, however the ΔT_{max} variations are far less due to the gradient being dominated by the tab heat generation rate in the positive tab. This highlights that methods to increase the heat removal from the large faces of the cell may increase the temperature gradient due to the low thermal conductivity of k_x.

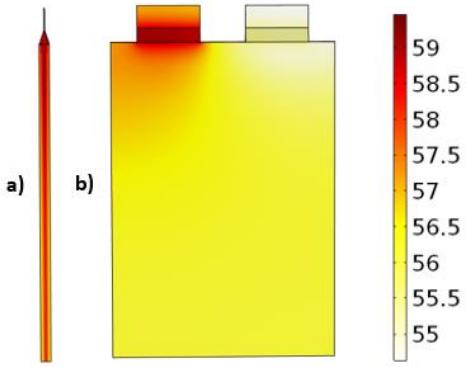

Figure 6: 8C cell temperature profile at t_{final} for cooling Case 4 (a) side view at positive tab side (b) back view of cell

4 Conclusion

Simulation results obtained from the electrochemical-thermal model indicate that minimal cooling strategies relying on natural convection of air to cool the cell are inadequate in limiting the peak cell temperature rise to below 20 ℃ when subject to an extreme duty profile. Under natural convection, the cell temperature gradient during the duty cycle is more influenced by heat rejection from the positive tab similar to that during the 8C discharge, with the cell thermal condition benefiting slightly from uneven tab cooling. For the 3C

discharge, the cell temperature gradient is worsened from uneven tab cooling owing to the much lower heat rejection rate into the cell from the tabs. In all cases the maximum cell temperature gradient remains below 5 ℃.

More involved thermal management strategies that increase the heat transfer rate from the large surfaces of the cell (front and back) are required to further reduce the volume averaged temperature of the cell to more acceptable levels (<<40 ℃). This necessitates a degree of spacing between cells to accommodate a heat removal mechanism. Further study is required to asses which mechanism may be appropriate given constraints on the battery maximum temperature, maximum temperature gradient, pack level energy density, weight and parasitic power requirement for achieving the heat transfer.

Acknowledgements

The research presented within this paper is supported by the Engineering and Physical Science Research Council (EPSRC - EP/ I01585X/1, EPSRCEP/M507593/1). The research was undertaken in collaboration with the WMG Centre High Value Manufacturing Catapult (funded by Innovate UK) in collaboration with Thermacore Europe, Jaguar Land Rover and Delta Motorsport.

References

[1] J. P. Lee, Peater K.;Chung, Youngwoo; OK, Tj;Hwang, KJ;Kim, Jaekyung;Jin, Matt;Park, "Global EV boom – revving up for the next upturn," no. August, 2014.
[2] J. Matthey, "Our Guide to Batteries," pp. 1–24, 2012.
[3] M. Anderman, "The Tesla Battery Report Outline," 2014.
[4] A. Tourani, P. White, and P. Ivey, "Analysis of electric and thermal behaviour of lithium-ion cells in realistic driving cycles," *J. Power Sources*, vol. 268, pp. 301–314, 2014.
[5] Y. Troxler, B. Wu, M. Marinescu, V. Yufit, Y. Patel, A. J. Marquis, N. P. Brandon, and G. J. Offer, "The effect of thermal gradients on the performance of lithium-ion batteries," *J. Power Sources*, vol. 247, pp. 1018–1025, 2014.
[6] T. Waldmann, M. Wilka, M. Kasper, M. Fleischhammer, and M. Wohlfahrt-Mehrens, "Temperature dependent ageing mechanisms in Lithium-ion batteries – A Post-Mortem study," *J. Power Sources*, vol. 262, pp. 129–135, 2014.
[7] M. Dubarry and B. Y. Liaw, "Identify capacity fading mechanism in a commercial LiFePO4 cell," *J. Power Sources*, vol. 194, no. 1, pp. 541–549, 2009.
[8] G. K. A. Pesaran , S.Santhanagopalan, "Addressing the Impact of Temperature Extremes on Large Format Li-Ion Batteries for Vehicle Applications," in *30TH INTERNATIONAL BATTERY SEMINAR*, 2013.
[9] T. M. Bandhauer, S. Garimella, and T. F. Fuller, "A Critical Review of Thermal Issues in Lithium-Ion Batteries," *J. Electrochem. Soc.*, vol. 158, p. R1, 2011.
[10] M. Fleckenstein, O. Bohlen, M. a. Roscher, and B. Bäker, "Current density and state of charge inhomogeneities in Li-ion battery cells with LiFePO4 as cathode material due to temperature gradients," *J. Power Sources*, vol. 196, no. 10, pp. 4769–4778, 2011.
[11] N. Yang, X. Zhang, B. Shang, and G. Li, "Unbalanced discharging and aging due to temperature differences among the cells in a lithium-ion battery pack with parallel combination," *J. Power Sources*, vol. 306, pp. 733–741, 2016.
[12] S. Chacko and Y. M. Chung, "Thermal modelling of Li-ion polymer battery for electric vehicle drive cycles," *J. Power Sources*, vol. 213, pp. 296–303, 2012.
[13] L. Song and J. W. Evans, "Electrochemical-Thermal Model of Lithium Polymer Batteries," *J. Electrochem. Soc.*, vol. 147, no. 6, p. 2086, 2000.
[14] M. Xiao and S.-Y. Choe, "Dynamic modeling and analysis of a pouch type LiMn2O4/Carbon high power Li-polymer battery based on electrochemical-thermal principles," *J. Power Sources*, vol. 218, pp. 357–367, 2012.
[15] G. Vertiz, M. Oyarbide, H. Macicior, O. Miguel, I. Cantero, P. Fernandez de Arroiabe, and I. Ulacia, "Thermal characterization of large size lithium-ion pouch cell based on 1d electro-thermal model," *J. Power Sources*, vol. 272, pp. 476–484, 2014.
[16] A. a Pesaran, "Battery Thermal Management in EVs and HEVs : Issues and Solutions," *Adv. Automot. Batter. Conf.*, p. 10, 2001.
[17] E. Schuster, C. Ziebert, A. Melcher, M. Rohde, and H. J. Seifert, "Thermal behavior and electrochemical heat generation in a commercial 40 Ah lithium ion pouch cell," *J. Power Sources*, vol. 286, pp. 580–589, 2015.
[18] U. S. Kim, J. Yi, C. B. Shin, T. Han, and S. Park, "Modelling the thermal behaviour of a lithium-ion battery during charge," *J. Power Sources*, vol. 196, no. 11, pp. 5115–5121, 2011.
[19] C. Veth, D. Dragicevic, and C. Merten, "Thermal characterizations of a large-format lithium ion cell focused on high current discharges," *J. Power Sources*, vol. 267, pp. 760–769, 2014.
[20] U. Seong Kim, J. Yi, C. B. Shin, T. Han, and S. Park, "Modeling the Dependence of the Discharge Behavior of a Lithium-Ion Battery on the Environmental Temperature," *J. Electrochem. Soc.*, vol. 158, no. 5, p. A611, 2011.
[21] R. Zhao, J. Gu, and J. Liu, "An experimental study of heat pipe thermal management system with wet cooling method for lithium ion batteries," *J. Power Sources*, vol. 273, pp. 1089–1097, 2015.
[22] M. Zolot, A. a. Pesaran, and M. Mihalic, "Thermal Evaluation of Toyota Prius Battery Pack," *SAE Int.*, no. 2002–01–1962, 2002.
[23] M. Xiao and S. Y. Choe, "Theoretical and experimental analysis of heat generations of a pouch type LiMn2O4/carbon high power Li-polymer battery," *J. Power Sources*, vol. 241, pp. 46–55, 2013.
[24] D. Bernardi, "A General Energy Balance for Battery Systems," *J. Electrochem. Soc.*, vol. 132, no. 1, p. 5, 1985.
[25] B. Wu, Z. Li, and J. Zhang, "Thermal Design for the Pouch-Type Large-Format Lithium-Ion Batteries: I. Thermo-Electrical Modeling and Origins of Temperature Non-Uniformity," *J. Electrochem. Soc.*, vol. 162, no. 1, pp. A181–A191, 2014.
[26] K. Shah, S. J. Drake, D. a. Wetz, J. K. Ostanek, S. P. Miller, J. M. Heinzel, and a. Jain, "Modeling of steady-state convective cooling of cylindrical Li-ion cells," *J. Power Sources*, vol. 258, pp. 374–381, 2014.
[27] Q. Kellner, W. D. Widanage, and J. Marco, "Battery Power Requirements in High-Performance Electric Vehicles," in *IEEE iTEC-2016*, 2016.
[28] T. Schoukens, J Dobrowiecki, "Design of broadband excitation signals with a user imposed power spectrum and amplitude distribution," in *IEEE Instrumentation and Measurement Technology Conference*, 1998, pp. 1002–1005.
[29] T. Bergman, A. Lavine, F. Incropera, and D. Dewitt, *Fundamentals of Heat and Mass transfer*. Chicago: John Wiley & Sons, 2011.
[30] S. J. Bazinski and X. Wang, "Thermal Effect of Cooling the Cathode Grid Tabs of a Lithium-Ion Pouch Cell," *J. Electrochem. Soc.*, vol. 161, no. 14, pp. A2168–A2174, 2014.